APPLICATION OF LIE GROUP ANALYSIS IN MAGNETO-TANGENT HYPERBOLIC FLUID FLOW OVER A POROUS ELONGATED SHEET WITH TEMPERATURE-RELIANT THERMAL CONDUCTIVITY

***Esan O.A., Ogunbayo T.O., Enobabor O.E., Ayeni O.M., Olusan B.O., and Amusa I.S.**

Department of Mathematics, Yaba College of Technology, Yaba, Nigeria.
*Corresponding author: olumide.esan@yabatech.edu.ng

Manuscript received 27/09/22 and accepted 26/10/22

ABSTRACT

An investigation of an electrically conducting hyperbolic tangent fluid motion along a porous sheet which stretches vertically upward with temperature-reliant thermal conductivity was scrutinized in this study. The current model characterizes thermal radiation and the impact of internal heat source in the heat equation plus velocity and thermal slipperation at the wall. The translation of the transport equations was carried out via the scaling Lie group technique and the resultant equations were numerically tackled by means of shooting method plus Runge-Kutta Fehlberg integration scheme. The results were publicized through various graphs to showcase the reactions of the parameters on the thermal and velocity fields. From these investigations, it was found that escalating values of the material Weissenberg number, slip and suction terms depleted the hydrodynamic boundary film whereas the heat field improved directly with thermal conductivity.

Keywords Magneto-Tangent Hyperbolic Fluid; Thermal conductivity; Porous sheet; Scaling Lie group; Thermal radiation.

1 INTRODUCTION

Magnetohydrodynamic is the interaction of an electromagnetic field with conducting fluids. Rheostat flow kinematics is a realistic application of magnetohydrodynamic where a magnetic field is used in conventional fluids since the heat exchange rate is unavailable for some sheet materials. Other uses include; thermal insulation, power storage, and so on. In the light of this, Abbas et al. (2020) investigated a lateral stretching sheet of MHD power-law fluid with differing thermal conductivity. The authors reported a shrinking boundary layer structure with growth in the magnetic field term at all phase of fluid categories considered in the report. Moreso, Azimi et al. (2012) analyzed magnetohydrodynamic viscous fluid flow across a nonlinear stretching sheet where the governing ordinary differential equation of the system was solved using the Pade-approximation. Jat *et al.* (2013) explored the viscous fluids heat transport and magnetohydrodynamic flow across an exponentially stretching layer accounting for viscous dissipation and radiation effect. Nadeem et al. (2015) explored the Magnetohydrodynamic rheological fluid flow on an angular boundary layer flow. The analysis showed that a rise in the magnetic field strength, the regular and tangential velocity profiles diminish while the skin friction coefficient increase.

Meanwhile, the studies conducted on the flow along a stretching sheet has become a great deal of interest among researchers in respect of significant contributions in manufacturing and engineering activities. Sakiadis (1961) analyzed the continuously moving flat surface on a laminar boundary layer and obtained a computational solution for the boundary layer equations. Crane (1970) extended this by reporting on the time-independent linearly stretching flow and specified the solution in a closed form. Such a study was also extended by Wang (2002) by incorporating partial slip effect whereas Nazarn et al. (2004) investigated

such a concept over a flat stretchable sheet when the flow is initiated spontaneously from rest. Hayat et al. (2011) analyzed slip fluid motion confined in a permeable stretchable material while the impact of partial slip due to vertical stretching sheet on stagnation-point flow with thermal transport was assessed by Zaimi and Ishak (2016). Babu and Sandeep (2016) examined the cross-diffusion impact on magnetohydrodynamic fluid flow through a stretched sheet with velocity slip. A case of MHD dissipative fluid flow occasioned by a nonlinearly stretched material with heat-mass transfer was numerically evaluated by Mabood et al. (2015). It was pointed out from the analysis that the thermal field is enlarged by the enhancement of the magnetic field. Such an investigation was also extended to the transport of Casson fluid configured in a three-dimensional sheet with pores and Joule heating effect by Sreenivasulu et al (2019) while Fatunmbi and Okoya (2020) inspected hydromagnetic micropolar fluid thermal transport characteristics over a stretching material featuring the prescribed surface temperature and prescribed heat flux wall heating conditions.

The studies of non-Newtonian fluids have inspired scientists and engineers in recent times owing to its many uses in science and technology including food processing, drug and pharmaceutical productions, chemical engineering works, etc. Examples of non-Newtonian fluids include gels, paints, blood, printers ink, lubricants with polymer ingredients, cosmetics and toiletries. Among various non-Newtonian fluid theories, there exists the tangent hyperbolic fluid model commonly utilized in numerous laboratory and chemical engineering processes. This fluid model displays a shear thinning attributes such that there exists a decline in the viscosity as the shear rate rises. This unique feature of tangent hyperbolic fluid makes it a sought after in bio-engineering operations, for instance, the thinning attributes of blood flow in the body serves as a prevention to the obstruction of arteries and veins such that coagulation effect is minimized (Jabeen et al., 2019).

In view of such striking characteristics, various researchers have applied this fluid model to analyze various flow problems under different configurations. Mamatha et al. (2018) investigated the motion of magnetohydrodynamic tangent hyperbolic fluid mixed with dust particles over a porous stretching plate with convective heating situation at the wall. A numerical evaluation of such a phenomenon towards a stagnation-point in the existence of thermal radiation, nonlinear convection, haphazard motion and thermo-migration of nanoparticles was scrutinized by Khan et al. (2018). Meanwhile, the transport of such a fluid with nanomaterials mixture over a nonlinear stretchable material was scrutinized by Fatunmbi et al. (2020) in the neighbourhood of a stagnation-point. These researchers reported a rise in the viscous drag due to enhancement in the power-law index and magnetic field terms. Oyelakin and Sibanda (2020) inspected the impact of exponentially based viscosity on the motion of hyperbolic tangent fluid. The report showed that a decrease in the viscosity triggered a spike in the velocity while lowering the heat and species intensity.

Sophius Lie (1976) found point metamorphosis that mapped a given differential equation and introduced the Lie group analysis classical approach. This approach brings together nearly every known technique of exact integration for all the associated ordinary and partial differential equations (Mehmet and Muhammet, 1988). Many researchers employed this technique to determine the similarities among given differential equations. Using this technique, the number of variables that control the partial differential systems can be effectively reduced. The dilution of values transforms the partial differential system into ordinary systems. Using Lie group analysis approach, convective dynamics problems have been studied on different flow configurations in

various science and engineering branches (Zakir and Zaman, 2017). Similarly, Ullah and Zaman (2017) engaged this approach while studying the transport and thermal effects of a tangent hyperbolic fluid past a stretched plate with Navier slip effect. Further, Ullah et al. (2020) engaged this approach to extend the work of Ullah and Zaman (2017) by incorporating suction/injection coupled with heat generation. Mina et al. (2021) examined the partial differential equations representing a natural convective unstable flow movement using the lie symmetry transformation approach. The classical Lie group transformation is applied twice sequentially in this study to transform the transport equations into a set of ordinary differential equations.

The above studies however ignored the impact of variable thermal conductivity in the thermal field. Thermal conductivity describes the characteristic quantity of fluids that allows them to conduct heat. For accurate prediction of heat transfer processes, the influence of temperature-based thermal conductivity has to be considered. Chiam (1988) investigated such an effect on a viscous fluid in the existence of a stretching layer by utilizing the shooting process and the perturbation procedure in analyzing the numerical solution. Similarly, Rangi et al. (2012) took into account the case of a stretching cylinder, considered a viscous fluid flow alongside variable thermal conductivity. The investigation depicted that growing the curvature of the cylinder causes the fluid temperature to rise rapidly. An examination of temperature based thermal conductivity coupled with thermal radiation impact of a viscous fluid in a porous stretching material was evaluated by Cortell (2012). Mat et al. (2013) reported on power-law mixed convection MHD fluid flow across a linearly stretching sheet alongside thermal conductivity influence. Recently, such a concept has been widely investigated by various researchers (Aziz and Shams, 2020) on diverse flow configurations and conditions.

In view of the discussion above and the consequential applications of essential fluids parameters in manufacturing and engineering works motivated the study, the current research is aimed to evaluate the motion and heat transfer of hydromagnetic tangent hyperbolic fluid over a porous vertical stretching sheet using Lie group analysis approach. In particular, this study extends that of Ullah and Zaman (2017) and Ullah et al. (2020) by considering porous medium with the inclusion of variable thermal conductivity, thermal radiation and a buoyancy effect which were ignored by previous authors. The essential of the thermofluid terms in thermal engineering and chemical science inspired the study. A unique similarity transformation approach is developed using the Lie group analysis which is adopted for transforming the nonlinear partial differential transport equations into a more simplified ordinary differential equation form. The resultant set of outlining equations is numerically tackled using the shooting algorithm in conjunction with Runge-Kutta Fehlberg integration scheme. The physical characteristics of dimensionless parameters obtained are clarified using graphs with appropriate discussion.

2 Problem Formulation Analysis

The underlisted assumptions have been identified as crucial for the formulation of the governing equations for the current investigation. Is is assumed that the fluid movement is time-independent, incompressible tangent hyperbolic fluid. The fluid movement is designed in a two-dimensional porous plate which stretches upwardly in a vertical route as portrayed in figure 1. The flow is routed in x axis while y axis runs normal to x axis. A restriction is placed on the flow in the region $y > 0$. There is slipperation in velocity and thermal boundary layers. There is a surface mass flux on the sheet surface having a velocity of $v_w(x)$ as expressed in Eq. (7). With the imposition of an external magnetic field

normal to x direction but ignoring that of the induced magnetic filed influence and electric field as well. Likewise, it is supposed that the radiative heat flux is negligible towards the x axis whereas it is applicable along y direction. Furthermore, the assumption of varying thermal conductivity is held valid with the inclusion of heat source. Other fluid attributes are are constant apart from the non-uniformity of the density in the body force in the momentum equation and the thermal conductivity. Boussinesq approximation coupled with boundary layer approximation are applied in this study for the derivation of the main equations.

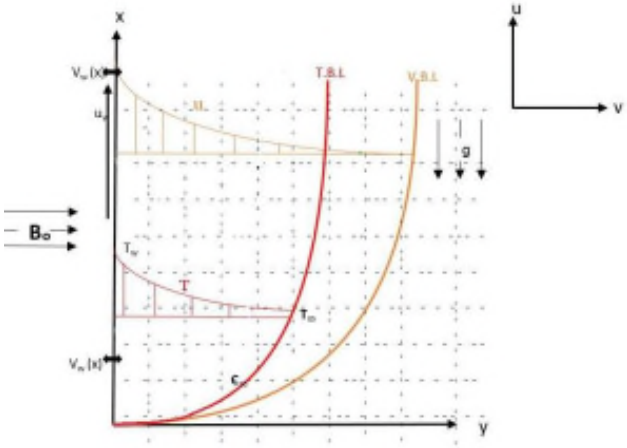


Figure 1 Flow configuration and coordinate system

For this study, the tangent hyperbolic fluid tensor is described as (Ullah and Zaman, 2017; Ullah et al., 2020)

$$\overline{\tau} = [\mu_\infty + (\mu_0 + \mu_\infty)\tanh(\Gamma\overline{\gamma})^m]\overline{\gamma}, \tag{1}$$

In Eq. (1), $\overline{\tau}$ describes stress tensor while μ_∞ depicts an infinite shear rate viscosity whereas μ_0 signifies the zero shear rate viscosity and Γ describes the time-dependent material constant whereas m connotes the power-law exponent while $\overline{\gamma}$ is expressed as:

$$\overline{\gamma} = \left(\frac{1}{2}\Sigma_i\Sigma_j\overline{\gamma}_{ij}\overline{\gamma}_{ji}\right)^{\frac{1}{2}} = \left(\frac{1}{2}\Pi\right)^{\frac{1}{2}}. \tag{2}$$

In Eq. (2), $\Pi = \frac{1}{2}tr((\nabla V)^T + \nabla V)^2$. The case $\mu_\infty = 0$ is accounted for owing to low influence of viscosity at infinity. Also taking into account the tangent hyperbolic fluid detailing shear thinning characteristics, with the assumption that $\Gamma\overline{\gamma} < 1$, Eq. (1) then reduces to:

$$\overline{\tau} = \mu_o[\Gamma\overline{\gamma}^m]\overline{\gamma} = \mu_o[(1 + \Gamma\overline{\gamma} - 1)^m]\overline{\gamma}$$

$$\approx \mu_o[(1 + m(\Gamma\overline{\gamma} - 1))]\overline{\gamma} \tag{3}$$

2.1 The Governing Equations

Combining the above-mentioned assumptions for the development of the transport model, Eqs. (4-6) describes the transport equations for the present investigation (see Khan et al., 2017; Ullah and Zaman, 2017; Ullah et al., 2020).

$$\frac{\partial u}{\partial x} + \frac{\partial v}{\partial y} = 0, \tag{4}$$

$$u\frac{\partial u}{\partial x} + v\frac{\partial u}{\partial y} = (1-m)\nu\frac{\partial^2 u}{\partial y^2} + \sqrt{2}\nu m\Gamma\left(\frac{\partial u}{\partial y}\right)\frac{\partial^2 u}{\partial y^2} - \frac{\sigma B^2}{\rho}u + g\beta_T(T - T_\infty) - \frac{\nu}{k_p}u, \tag{5}$$

$$u\frac{\partial T}{\partial x} + v\frac{\partial T}{\partial y} = \frac{1}{\rho C_p}\frac{\partial}{\partial y}\left(k(T)\frac{\partial T}{\partial y}\right) - \frac{1}{\rho C_p}\frac{\partial q_r}{\partial y} + \frac{Q_o}{\rho C_p}(T - T_\infty). \tag{6}$$

The respective boundary conditions for the governing equations are stated below

$$u = cx + \beta\frac{\partial u}{\partial y},\ v = v_w(x),\ T = T_w + G\frac{\partial T}{\partial y}\ \ at\ \ y = 0, \tag{7}$$

$$u \longrightarrow 0, T \longrightarrow T_\infty\ \ as\ \ y \longrightarrow \infty. \tag{8}$$

The radiative heat flux q_r in Eq. (6) is indicated in Eq. (9) as (see Sumalatha and Bandari, 2015)

$$q_r = -\left(\frac{4\sigma^*}{3k^*}\right)\frac{\partial T^4}{\partial y} \tag{9}$$

From the above Eqs.(4-9), u and v describe velocity components in respect to x and y axes. The symbols k_p, β and σ represent porous medium permeability, velocity slip factor and electrical conductivity whereas the density, volumetric thermal expansion coefficient, magnetic flux density and the thermal slip factor are sequentially denoted by ρ, β_T, B and G. Also, T signals the fluid temperature, g denotes gravitational acceleration, ν is the kinematic viscosity, v_w describes surface mass flux, c defines stretching rate and Q_o describes coefficient of heat source/sink, σ^* connotes Stefan-Boltzmann constant while the mean absorption coefficient is denoted by k^*. By the application of the Rosseland approximation and assuming that the temperature variation in the flow field is low such that Taylor's series can utilized to expand T^4 to get (see Fatunmbi and Fenuga, 2018)

$$T^4 \approx 4T_\infty^3 - 3T_\infty^4,$$

The temperature-based thermal conductivity is also specified as (see Animasaun, 2014):

$$k(T) = k_\infty[1 + \zeta(T - T_\infty)], \tag{10}$$

where k_∞ denotes the upstream thermal conductivity, ζ typifies the thermal conductivity parameter. To transform the outlining governing equations into dimensionless system, the underlisted dimensionless variables are introduced:

$$\frac{\overline{x}}{x} = \left(\frac{a}{\nu}\right)^{\frac{1}{2}},\ \frac{\overline{y}}{y} = \left(\frac{a}{\nu}\right)^{\frac{1}{2}},\ \frac{\overline{u}}{u} = \frac{1}{(av)^{\frac{1}{2}}},\ \frac{\overline{v}}{v} = \frac{1}{(av)^{\frac{1}{2}}},\ T = (T_w - T_\infty)\theta + T_\infty. \tag{11}$$

Dropping the bar and substituting $u = \frac{\partial\psi}{\partial y}$ and $v = -\frac{\partial\psi}{\partial x}$ into Eqs. (5-6) taking cognizance Eqs (9) and (10), the underlisted are obtained

$$\left(\frac{\partial\psi}{\partial y}\frac{\partial^2\psi}{\partial x\partial y} - \frac{\partial\psi}{\partial x}\frac{\partial^2\psi}{\partial y^2}\right) = (1-m)\frac{\partial^3\psi}{\partial y^3} + \sqrt{2}ma\Gamma\left(\frac{\partial^2\psi}{\partial y^2}\right)\frac{\partial^3\psi}{\partial y^3} - \left(\frac{\sigma B^2}{a\rho} + \frac{\nu}{ak_p}\right)\frac{\partial\psi}{\partial y} + \frac{gB_T(T_w - T_\infty)}{a^{\frac{3}{2}}\nu^{\frac{1}{2}}}\theta, \tag{12}$$

$$\left(\frac{\partial\psi}{\partial y}\frac{\partial\theta}{\partial x} - \frac{\partial\psi}{\partial x}\frac{\partial\theta}{\partial y}\right) = \left(\frac{k_\infty}{\mu c_p}(1 + \zeta\theta) + \frac{16\sigma^*}{3\mu c_p k^*}T_\infty^3\right)\frac{\partial^2\theta}{\partial y^2} + \frac{k_\infty}{\mu c_p}\zeta\left(\frac{\partial\theta}{\partial y}\right)^2 + \frac{B_o}{a\rho C_p}\theta, \tag{13}$$

Also, the boundary conditions (7-8) transform to:

$$\begin{aligned} &\frac{\partial\psi}{\partial y} = \frac{c}{a}x + \beta\sqrt{\frac{a}{\nu}}\frac{\partial^2\psi}{\partial y^2}, \frac{\partial^2\psi}{\partial x^2} = \frac{v_w}{\sqrt{a\nu}}, \theta = 1 + G\sqrt{\frac{a}{\nu}}\frac{\partial\theta}{\partial y} \quad at \quad y = 0, \\ &\frac{\partial\psi}{\partial y} \to 0,\ \theta \to 0\ \ as\ \ y \to \infty. \end{aligned} \tag{14}$$

3 Lie Group Scaling Transformations

The Lie scaling technique depends on theory formulated to find all symmetry transformations that keep the system of equations unchanged. It helps in reducing the number of independent variables and in consequence transforms the PDEs to an ODEs. Using this method to generate similarity variables involves finding the invariant solution which does not alter the

structure of the given equation under study. In this section, the simplified format of the Lie group transformation approach known as the scaling group of transformations is employed to derive the new similarity transformations for the transport equations. In this case, the outlining partial differential equations can be converted into ordinary differential equations. Following Mukhopadhyay *et al.* (2005); Bhattacharyya et al. (2011) Ullah and Zaman (2017); Ullah et al. (2020), the underlisted scaling group of transformation is defined

$$\Upsilon: x^* = xe^{\varepsilon\gamma_1},\ y^* = ye^{\varepsilon\gamma_2},\ \psi^* = \psi e^{\varepsilon\gamma_3},\ \theta^* = \theta e^{\varepsilon\gamma_4},\ \Gamma^* = \Gamma e^{\varepsilon\gamma_5} \qquad (15)$$

In Eq. (15), ε depicts the parameter of the group whereas the transformation variables are represented by $\gamma_1, \gamma_2, \gamma_3, \gamma_4, \gamma_5$. Also, Eq. (15) is regarded as a point transformation by which the set of coordinates system $(x, y, \psi, \theta, \Gamma)$ transforms into $(x^*, y^*, \psi^*, \theta^*, \Gamma^*)$. The substitution of the transformation Eq. (15) into Eq. (12) and (13) results to the form:

$$e^{\varepsilon(\gamma_1+2\gamma_2-2\gamma_3)}\left(\frac{\partial\psi^*}{\partial y^*}\frac{\partial^2\psi^*}{\partial x^*\partial y^*} - \frac{\partial\psi^*}{\partial x^*}\frac{\partial^2\psi^*}{\partial y^{*2}}\right) = e^{\varepsilon(3\gamma_2-\gamma_3)}(1-m)\frac{\partial^3\psi^*}{\partial y^{*3}} + e^{\varepsilon(5\gamma_2-2\gamma_3-\gamma_5)}\left(\sqrt{2}m\Gamma\left(\frac{\partial^2\psi^*}{\partial y^{*2}}\right)\frac{\partial^3\psi^*}{\partial y^{*3}}\right)$$
$$-e^{\varepsilon(\gamma_2-\gamma_3)}\left(\frac{\sigma B^2}{a\rho} + \frac{\nu}{ak_p}\right)\frac{\partial\psi^*}{\partial y^*} + \frac{gB_T(T_w-T_\infty)}{a^{\frac{3}{2}}\nu^{\frac{1}{2}}}\theta^* e^{-\varepsilon\gamma_4}, \qquad (16)$$

$$e^{\varepsilon(\gamma_1+\gamma_2-\gamma_3-\gamma_4)}\left(\frac{\partial\psi^*}{\partial y^*}\frac{\partial\theta^*}{\partial x^*} - \frac{\partial\psi^*}{\partial x^*}\frac{\partial\theta^*}{\partial y^*}\right) = e^{\varepsilon(2\gamma_2-\gamma_4)}\left(\frac{k}{\mu c_p}(1+\zeta\theta^*) + \frac{16\sigma^*}{3\mu c_p k^*}T^3\right)\frac{\partial^2\theta^*}{\partial y^2} +$$
$$e^{\varepsilon(2\gamma_2-2\gamma_4)}\frac{k}{\mu c_p}\zeta\left(\frac{\partial\theta^*}{\partial y^*}\right)^2 + \frac{B_o}{a\rho C_p}\theta^* e^{-\varepsilon\gamma_4}. \qquad (17)$$

Similarly, the boundary conditions transform to:

$$e^{\varepsilon(\gamma_2-\gamma_3)}\frac{\partial\psi^*}{\partial y^*} = \frac{c}{a}e^{-\varepsilon\gamma_1}x^* + \beta\ \ \frac{\bar{a}}{\nu}\frac{\partial^2\psi^*}{\partial y^{*2}}e^{\varepsilon(2\gamma_2-\gamma_3)}, \frac{\partial^2\psi^*}{\partial x^{*2}}e^{\varepsilon(\gamma_2-\gamma_3)} = \frac{v}{\sqrt{av}},$$
$$e^{-\varepsilon\gamma_4}\theta^* = 1 + G\ \ \frac{\bar{a}}{\nu}\frac{\partial\theta^*}{\partial y^*}e^{\varepsilon(\gamma_2-\gamma_4)}\quad at\quad e^{-\varepsilon\gamma_1}y^* = 0, \qquad (18)$$
$$e^{\varepsilon(\gamma_2-\gamma_3)}\frac{\partial\psi^*}{\partial y^*} \to 0,\ e^{-\varepsilon\gamma_4}\theta^* \to 0\ as\ y^* \to \infty.$$

The preceding system of equations is invariant under the group transformation if the underlisted relationship exist among the exponents:

$$\gamma_1 + 2\gamma_2 - 2\gamma_3 = 3\gamma_2 - \gamma_3 = 5\gamma_2 - 2\gamma_3 - \gamma_5 = \gamma_2 - \gamma_3 = -\gamma_4 \qquad (19)$$

$$\gamma_1 + \gamma_2 - \gamma_3 - \gamma_4 = 2\gamma_2 - \gamma_4 = 2\gamma_2 - 2\gamma_4 = -\gamma_4 \qquad (20)$$

solving Eq. (19) and (20) to obtain the following relations:

$$\gamma_1 = \gamma_3, \gamma_2 = 0, \gamma_4 = \gamma_1, \gamma_5 = -\gamma_1 \qquad (21)$$

Eq. (21) can then be introduced into Eq. (15) to obtain one criterion set of transformations as:

$$\Upsilon: x^* = xe^{\varepsilon\gamma_1}, y^* = y, \psi^* = \psi e^{\varepsilon\gamma_1}, \theta^* = \theta, \Gamma^* = \Gamma e^{-\varepsilon\gamma_1} \qquad (22)$$

Applying Taylor's series to expand Eq. (22) in the power of ε to the first order to obtain:

$$x^* - x = x\varepsilon\gamma_1,\ y^* - y = 0,\ \psi^* - \psi\varepsilon\gamma_1,\ \theta^* - \theta = 0,\ \Gamma^* - \Gamma = -x\varepsilon\gamma_1, \qquad (23)$$

From Eq. (23), the following characteristic equation were obtained:

$$\frac{dx}{x\gamma_1} = \frac{dy}{0} = \frac{d\psi}{x\gamma_1} = \frac{d\theta}{0} = \frac{d}{-x\gamma_1}, \qquad (24)$$

the following similarity transformations are derived by solving Eq. (24) (see Ulla and Zaman, 2017):

$$\eta = y,\ \psi = xf(\eta),\ \theta = \theta(\eta),\ \Gamma = x^{-1}\Gamma_o \tag{25}$$

The non-dimensional ODEs obtained with corresponding boundary condition via the similarity transformations (25) into Eqs. (16-18) are as follows:

$$(1-m)f''' + mW_e f'''(f'') + ff'' - (M^2 + Da)f' - (f')^2 + Gr\theta' = 0 \tag{26}$$

$$(1 + \zeta\theta + Nr)\theta'' + \zeta\theta'^2 + Pr(Q\theta + f\theta') = 0 \tag{27}$$

$$f'(0) = \lambda + \alpha f''(0),\ f(0) = S,\ \theta(0) = 1 + \theta'(0), \tag{28}$$

$$f' \to 0,\ \theta \to 0 \quad as \quad \eta \to \infty. \tag{29}$$

In Eqs. (26-29), $W_e = \sqrt{2}a\Gamma$ symbolizes the Weissenberg number, $Nr = \frac{16\sigma^*}{3k^*k}T_\infty^3$ defines radiation parameter, $M^2 = \frac{\sigma B^2}{a\rho}$ denotes Hartmann number, $Q = \frac{Q_0}{a\rho c_p}$ typifies the heat source/sink factor and $b = \sqrt{\frac{a}{\nu}}G$ is the thermal slip parameters whereas $\alpha = \sqrt{\frac{a}{\nu}}\beta$ represents the velocity slip, $Da = \frac{\nu}{ak_p}$ characterizes the Darcy number and ζ implies thermal conductivity parameter. The primes signifies differential with respect to η, $\lambda = \frac{c}{a}$ is the stretching parameter, $Gr = \frac{gB_T(T_w - T_\infty)}{a^{\frac{3}{2}}\nu^{\frac{1}{2}}x}$ symbolizes the Grashof number, $S = \frac{v_w}{\sqrt{a\nu}}$ is the mass suction and $Pr = \frac{\mu c_p}{k_\infty}$ represents the Prandtl number. The incorporated quantities of engineering interest in the current investigation include the skin friction coefficient Cf_x and the Nusselt number Nu_x which are orderly specified in Eq. (30) as:

$$\rho(ax)^2 Cf_x = \tau_w,\ Nu_x = \frac{xq_w}{k(T_w - T_\infty)} \tag{30}$$

where

$$\tau_w = (1-m)\frac{\partial u}{\partial y} + \frac{m\Gamma}{\sqrt{2}}\left(\frac{\partial u}{\partial y}\right)^2\Big|_{y=0},\ q_w = -k_\infty\left(1 + \frac{16\sigma^*}{3k^*k_\infty}T_\infty^3\right)\frac{\partial T}{\partial y}\Big|_{y=0} \tag{31}$$

The dimensionless form of Eq. (30) are specified in Eq. (31) as:

$$Re^{\frac{1}{2}}C_f = [(1-m)f''(0) + \frac{m}{2}W_e(f''(0))^2],\ Re^{-\frac{1}{2}}Nu_x = -(1 + Nr)\theta'(0), \tag{32}$$

where $Re_x = \frac{ax^2}{\nu}$ signifies the local Reynolds number.

4 NUMERICAL SOLUTION

Eqs. (26-27) comprises of a set nonlinear coupled differential equations with it's associated wall conditions. Owing to the nonlinearity nature of the governing equations, Eqs (26-27) subject to (28-29) are tackled numerically using shooting techniques alongside Runge-Kutta Fehlberg integration technique by utilizing a computer algebra symbolic software (Maple). This algorithm relies on Runge-Kutta Fehlberg method alongside shooting technique. The numerical code's accuracy is validated by assessing the computational values of the skin friction coefficient C_{fx} obtained in this study as compared with previously published works of Akbar (2013) and Fathizadeh (2013) in respect to variations in the Hartmann number M. As recorded in Table 1, the comparison showed a perfect harmony with the existing data in the literature under limiting circumstances and thus confirming the accuracy of our numerical code.

Table 1 Skin friction coefficient as compared with previous studies when $W_e = m = 0$

M	Akbar (2013)	Fathizadeh (2013)	Present values
0	1.00000	1.00000	1.00000
1	−1.41421	−1.41421	−1.41421
5	−2.44948	−2.44948	−2.44949
10	−3.31662	−3.31662	−3.31663
50	−7.14142	−7.14142	−7.14143
100	10.0499	10.0499	10.0499
500	−22.38300	−22.38300	−22.38300

5 RESULTS AND DISCUSSION

This section displays and discusses the reactions of the dimensionless velocity and temperature profiles due to variations in the physical flow parameters. These physical parameters include the stretching parameter (λ), Grashof number (Gr), Prandtl number (Pr), Weissenberg number (We), Darcy number (Da), heat source term (Q), power-law exponent term (m), velocity slip term (α), radiation parameter (Nr), Hartmann number (M), mass suction parameter (S), thermal conductivity parameter (ζ), and temperature slip term (b).

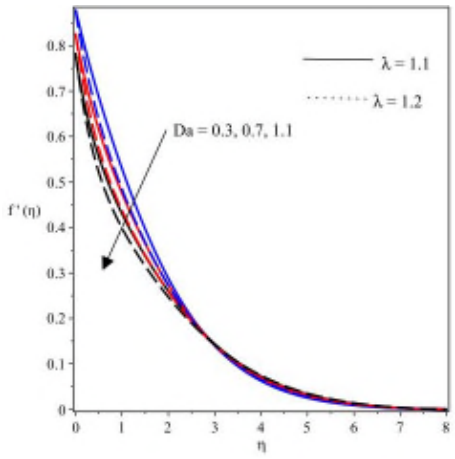


Fig. 2 Impact of Da & λ on velocity $f'(\eta)$

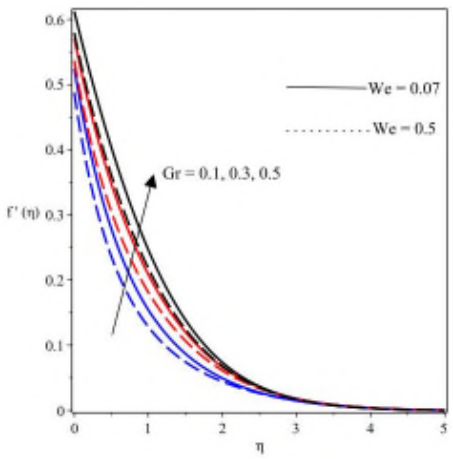


Fig. 3 Behaviour Gr & We on velocity $f'(\eta)$

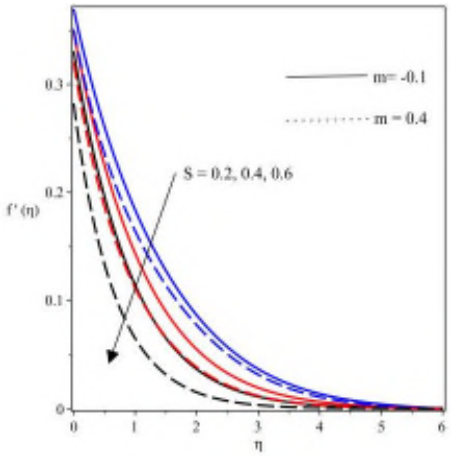


Fig. 4 Effect of S & m on velocity $f'(\eta)$

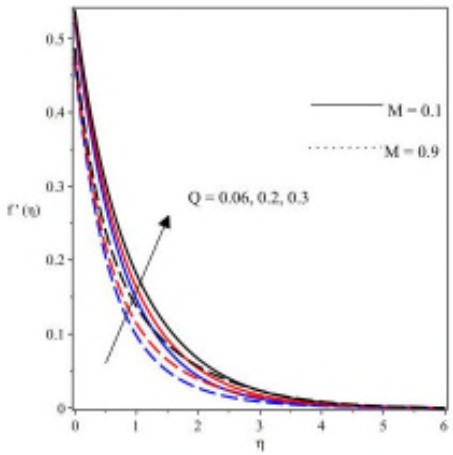


Fig. 5 Reaction Q & M on velocity $f'(\eta)$

Figures 2-6 describe the influences of various physical flow parameter on the velocity profile. Fig. 2 illustrates the effects of (Da) Darcy number on the dimensionless velocity in the existence of stretching parameter (λ). Evidently, there is a decrease in the velocity as Da increases. This trend occurs due to the fact that a spike in Darcy number (Da) creates a resistance in the flow field leading to a shrink boundary layer and thereby decelerates the fluid motion. In a related sense, an enhancement in the magnitude of the stretching parameter (λ) lowers the momentum boundary layer structure and consequently decelerates the locomotion. The impacts of Grashof number (Gr) and Weissenberg number (We) on the dimensionless velocity profile are presented in Fig. 3. It is evident from the graph displayed that the velocity drop significantly by a rise in (We) owing to an increase in the viscosity whereas there is an acceleration in the fluid motion as Grashof number increases due to enhancement in the buoyancy force. As Gr is raised, the buoyancy force dominates the viscous force and thus encourages a boost in the velocity. Fig. 4 portrays the influence of mass suction parameter (S) coupled with that of the power-law index (m) on the profile of velocity. It is evident that enhancing the magnitude of the power-law index (m) leads to a rise in viscosity and as a result, there is a significant drop in fluid velocity. Also, this plot shows that with an increase in the magnitude of S and m, the hydrodynamic boundary structure thickness declines and the velocity decelerates. The evaluation of the heat source (Q) term and the Hartmann number (M) is plotted in Fig. 5. Evidently, the action of the Lorentz force produced by the interaction of the magnetic field and the electrically conducting tangent hyperbolic fluid creates a drag in the fluid motion as noted in this figure. The electroconducting fluid's interaction with the transverse magnetic field induces a retarding force on the fluid motion. Similarly, a hike in Q induces higher flow rate in the velocity field due to reduction in the viscosity. Fig. 6 demonstrates the behaviour of (α) on the fluid motion. In this plot, a declining trend is observed in the velocity profile as the slip parameter α rises

.

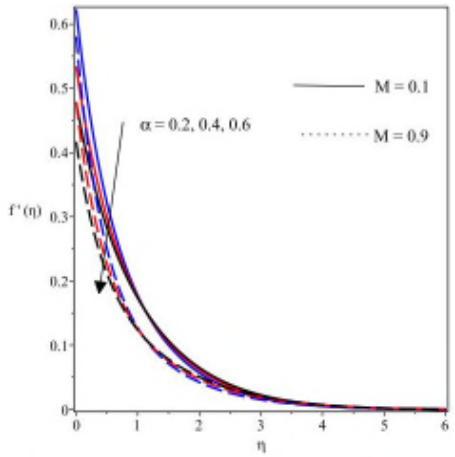


Fig. 6 Impact of α & M on velocity $f'(\eta)$

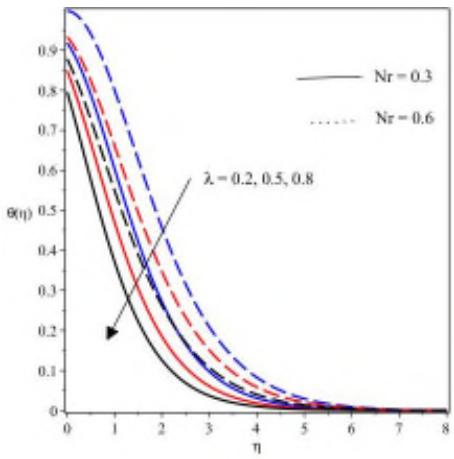


Fig. 7 Impact of λ & Nr on temperature $\theta(\eta)$

Figures 7-12 describe the variations of some physical parameters on the field of temperature. Firstly, the temperature profile showing the impact of λ in the presence of thermal radiation Nr parameter is plotted in Fig 7. The graph elucidates that advancement in λ causes the temperature to fall whereas growing Nr enhances the thermal profile. An advancement in the radiative heat flux corresponding to a rise in Nr while the Rosseland mean absorption coefficient declines and as such, the thermal field is enhanced as found in this figure. The results of the Prandtl number (Pr) and power-law index (m) on the temperature profile are depicted in Fig. 8. The graph demonstrates that an increment in Pr lowers the thermal field by shrinking the thermal boundary layer structure whereas the temperature distribution improves as m rises. The Prandtl number connotes the ratio of momentum diffusivity to the thermal diffusivity and also influence the relative thickness of the momentum and thermal boundary layers. Thus, a rise in Pr implies a reduction in the thermal boundary layer and consequently leads to a decline in the temperature. The reactions of heat source parameter (Q) and Hartmann number (M) on the temperature distribution are displayed in Fig. 9. The graph portrays the fluid temperature exhibiting identical growing patterns on Q and M. Typically, both parameters cause a rising trend in the thermal boundary layer. An enhancement in M induces a higher Lorentz force which creates an obstruction to the fluid motion and thus increase frictional heating effect which boosts the surface temperature. Similarly, a hike in Q is an indication of extra energy being generated and thus, a rise in the temperature as found in this figure.

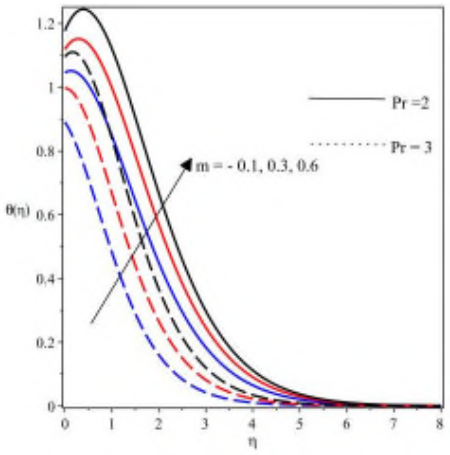


Fig. 8 Reactions of m & Pr on temperature $\theta(\eta)$

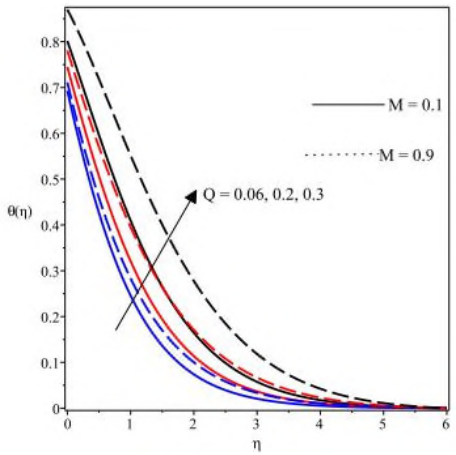


Fig. 9 impact of Q & M on temperature $\theta(\eta)$

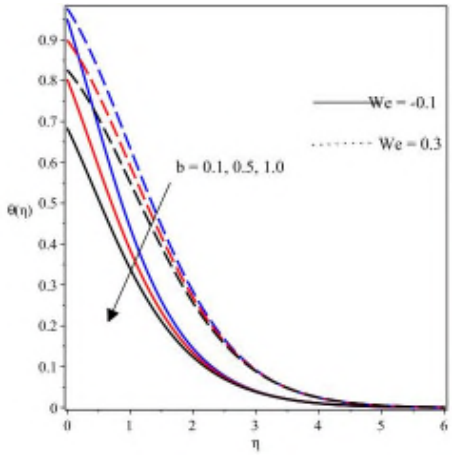


Fig. 10 Impact of b & We on temperature $\theta(\eta)$

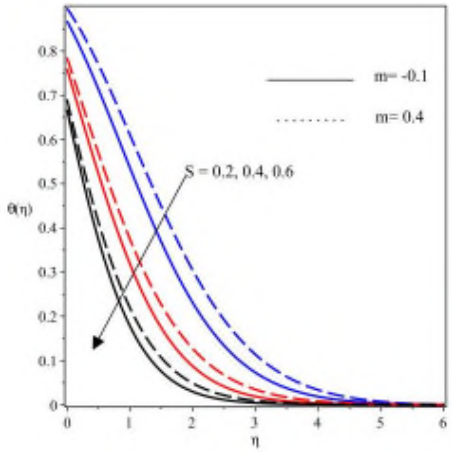


Fig. 11 Effect of S & m on $\theta(\eta)$

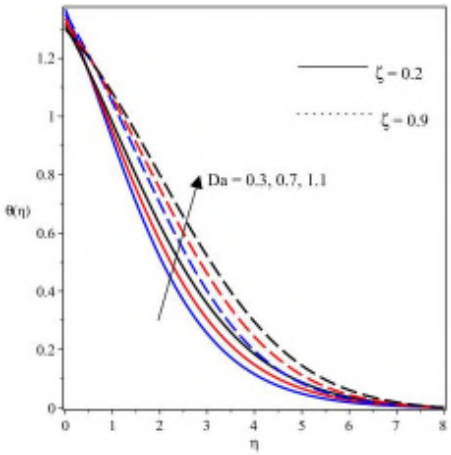


Fig. 12 Influence of Da & ζ on temperature $\theta(\eta)$

Fig. 10 elucidates the reactions of the thermal slip parameter (b) and Weissenberg number (We) on the fluid temperature profile. The thermal boundary structure shrinks and the temperature falls with growth in b whereas the converse occurs with enhancement in We as noticed in this figure. A rise in b draws away the fluid from the heated region thereby lowers the temperature whereas as We rises in

magnitude a frictional heat is generated due to rising viscosity. The reactions of mass suction term (S) and power-law index (m) are plotted in Fig. 11. This plot reveals that with advancement in S, the temperature distribution subsides whereas as m increases, the temperature distribution shoots up. Likewise, the plot showing the variation in Darcy term Da and thermal conductivity term ζ in respect to temperature is sketched in Fig. 12. It is noticeable that an increment in the (Da) and ζ boost the temperature distribution due to extra heat generated by the resistance imposed on the fluid flow as Da increases.

6 CONCLUSION

A numerical analysis has been performed on the motion and heat transfer of magnetohydrodynamic tangent hyperbolic fluid passing a vertically stretched surface with varying thermal conductivity. The flow is configured in a steady two-dimensional and incompressible stretchable sheet enclosed in a porous medium with the impact of thermal radiation and internal heat source. Lie group analysis generates the similarity transformation which transformed the coupled differential equations with boundary conditions from partial to ordinary differential equations, The main equations are then solved numerically via shooting approach alongside Runge-Kutta Fehlberg method. The solutions are presented graphically and deliberated while comparison with published studies show good agreement. The study also reveals that:

• The fluid velocity accelerates with enhancement in the magnitude of Grashof number Gr and heat source term Q. However, augmenting the magnitude of the Darcy number Da, suction S term, velocity slip α, stretching term λ, Hartmann number M, power-law index m as well as Weissenberg number We decelerates the velocity profile.

• There is a fall in thermal boundary structure and the corresponding surface temperature distribution falls with a rise in the mass suction parameter S, Prandtl number Pr and thermal slip parameter b.

• A thicker thermal boundary layer structure is formed with advancing magnitude of the thermal conductivity parameter ζ, thermal radiation term Nr, Darcy number as well as the heat source parameter Q.

The study can be further extended to other viscoelastic fluid flows with binary chemical reaction in an annular cylinder and thin needle.

REFERENCES

Abbas, T., Rehman, S., Muhammad, A. S., Utmankhel, I. (2020). Analysis of MHD Carreau fluid flow over a stretching permeable sheet with variable viscosity and thermal conductivity. Physica A: Statistical Mechanics Applications, 551, 215-225.

Abel, M. S., Siddheshwar, P. G., Mahesha, N. (2009). Effects of thermal buoyancy and variable thermal conductivity on the MHD flow and heat transfer in a power-law fluid past a vertical stretching sheet in the presence of a non-uniform heat source. International journal of non-linear mechanics, 44, 1-12.

Afify, A., Abd-el-azizi, M. (2017). Lie group analysis of ?ow and heat transfer of non-Newtonian nano?uid over a stretching surface with convective boundary condition. Journal of Physics, 88(31): doi:10.1007/s12043-016-1336-1.

Akbar, N. S, Nadeem, S., Haq, R. U., Khan, Z. H. (2013). Numerical solutions of Magnetohydrodynamic boundary layer flow of tangent hyperbolic fluid towards a stretching sheet. Indian Journal of Physics, 87(11):1-4.

Animasaun, I. L. (2014). Effects of thermophoresis, variable viscosity and thermal conductivity on free convective heat and mass transfer of non-Darcian MHD dissipative

Casson fluid flow with suction and nth order of chemical reaction, Journal of Nigeria Mathematical Society, 2014, 1-21.

Azimi, M., Ganji, D. D., Abbassi, F. (2012). Study on MHD viscous flow over a stretching sheet using DTM-Pade technique, Modern Mechanical Engineering, 2: 126-129.

Aziz, Z. and Shams, M. (2020). Entropy generation in MHD Maxwell nanofluid flow with variable thermal conductivity, thermal radiation, slip conditions, and heat source, AIP Advances 10, 015038 (2020); doi: 10.1063/1.5129569

Babu, M. J., Sandeep, N. (2016). MHD non-Newtonian fluid flow over a slendering stretching sheet in the presence of cross-diffusion effects. Alexandria Engineering Journal, 55, 2193-2201.

Bhattacharyya, K., Uddin, M. S. and Layek, G. C. (2011). Application of scaling group of transformations to steady boundary layer flow of Newtonian fluid over a stretching sheet in presence of chemically reactive species, *Journal of Bangladesh Academy of Sciences, 35*(1): 43-50.

Chiam, T. C. (1998). Heat transfer in a fluid with variable thermal conductivity over a linearly stretching sheet. Acta Mech., 129: 63-72.

Cortell, R. (2012). Heat transfer in a fluid through a porous medium over a permeable stretching surface with thermal radiation and variable thermal conductivity. Canadian journal of chemical engineering, 90: 1347-1355.

Crane, L. J. (1970). Flow past a stretching plane.Z. Angew. Math. Phys, 21, 645-647.

Fathizadeh, M., Madani, M., Khan, Y., Faraz, N., Tutkun, S. (2013). J. King. Saud. University Sci. doi:10.1016/j.jksus.2011.08.003

Fatunmbi, E. O., Fenuga, O. J. (2018). MHD micropolar fluid fow over a permeable stretching sheet in the presence of variable viscosity and thermal conductivity with Soret and Dufour effects. International Journal of Mathematical Analysis and Optimization: Theory and Application, 211- 232.

Fatunmbi, E. O and Okoya, S. S. (2020). Heat transfer in boundary Layer magneto-micropolar fluids with temperature-dependent material properties over a stretching sheet, Advances in Materials Science and Engineering Article ID 5734979, 1-11.

Goyal, M., Bhargava, R. (2013). Numerical solution of MHD viscoelastic nanofluid flow over a stretching sheet with partial slip and heat source/sink. ISRN Nanotechnology, http://dx.doi.org/10.1155/2013/931021.

Hayat, T., Qasim, M., Mesloub, S. (2011). MHD flow and heat transfer over permeable stretching sheet with slip conditions. Int. J. Numer. Methods Fluids, 66(8): 963-975.

Jabeen, S., Azam, Q., Hayat, T., Qayyum, S. and Alsaedi, A. (2019). Significance of activation energy in stratified flow of tangent hyperbolic fluid, International Journal of Numerical Methods for Heat & Fluid Flow, 29(6): 2932-2947.

Jat, R. N., Chand, G. (2013). MHD flow and heat transfer over an exponentially stretching sheet with viscous dissipation and radiation effects. Applied Mathematical Sciences, 7:167-180.

Khan, M., Hussain, A., Malik, M.Y., Salahuddin, T., Khan, F., (2017). Boundary layer flow of MHD tangent hyperbolic nanofluid over a stretching sheet: A numerical investigation, Results in Physics, doi: http://dx.doi.org/10.1016/j.rinp.2017.07.061

Khan, M. I., Tufail A. Khan, T. A., Qayyum1, S., Hayat, T., Khan4, M, M. and Alsaedi, A. (2019). Entropy generation optimization and activation energy in nonlinear mixed convection flow of a tangent hyperbolic nanofluid, Eur. Phys. J. Plus, 133: 1-20.

Lin, Y., Zheng, L., Chen, G. (2015). Unsteady flowand heat transfer of pseudo-plastic nanoliquid in a finite thin film on a stretching surface with variable thermal conductivity and viscous dissipation. Powder Technology, 274: 324-332.

Mabood, F., Khan, W. A. and Ismail, A.I.M. (2015). MHD boundary layer flow and heat transfer of nanofluids over a nonlinear stretching sheet: A numerical study, Journal of Magnetism and Magnetic Materials, 374: 569-576

Malik, M. Y., Khan, I., Hussain, A., Salahuddin, T. (2015). Mixed convection flow of MHD Eyring-Powell nanofluid over a stretching sheet. A numerical study AIP advances, 5: 117-118.

Mamatha, S. U., Raju, C.S. K., Mahesha and Makinde, O. D. (2018). Radiative and viscous ohmic dissipation on MHD tangent hyperbolic fluid over a convectively heated sheet in a suspension of dust particles, Diffusion Foundations, 16: 177-190.

Mat, N. A. A., Arifin, N. M., Nazar, R., Ismail, F., Bachok, N. (2013). MHD mixed convection flow of a power law nanofluid over a vertical stretching sheet with radiation effect. AIP conference proceedings, 1557, 604 .

Mukhopadhyay, S., Layek, G. C. and Samad S. A. (2005). Study of MHD boundary layer flow over a heated stretching sheet with variable viscosity, *International Journal of Heat and Mass Transfer, 48*: 4460-4466

Nadeem, S., Mehmood, R., Akbar, N. S. (2015). Combined effects of magnetic field and partial slip on obliquely striking rheological fluid over a stretching surface. Journal of magnetism and Magnetic Materials, 378: 457-462.

Oyelakin, I.S., Sibanda, P. (2020). Analysis of exponentially varying viscosity and thermal conductivity on a tangent hyperbolic fluid. SeMA, 77: 257-273.

Pakdemirli, M., Yurusoy, M. (1998). Similarity transformations for partial differential equations. SIAM Rev, 40(1): 96-101.

Rangi, R., Ahmad, N. (2012). Boundary layer flow past a stretching cylinder and heat transfer with variable thermal conductivity. Applied mathematics, 3:205-209.

Sakiadis, B. C. (1961). Boundary-layer behavior on continuous solid surfaces: I. Boundary-layer equations for two-dimensional and axisymmetric flow. AIChEJ, 7(1): 26-28.

Salahuddin, T., Malik, M. Y., Hussain, A., Bilal, S., Awais, M. (2015). MHD flow of Cattanneo-Christov heat flux model for Williamson fluid over a stretching sheet with variable thickness: Using numerical approach. Journal of Magnetism and Magnetic Materials, 401: 991-997.

Sari, G. Z., Pakdemirli, M., Hayat, T., Aksoy, Y. (2012). Boundary Layer Equations and Lie Group Analysis of a Sisko Fluid. Journal of Applied Mathematics, 259608(9), doi:10.1155/2012/259608.

Ullah, Z. and Zaman, G. (2017). Lie group analysis of magnetohydrodynamic tangent hyperbolic fluid flow towards a stretching sheet with slip conditions, Heliyon 3, e00443.

Ullaha, Z., Zamana, G. and Ishak, A. (2020). Magnetohydrodynamic tangent hyperbolic fluid flow past a

stretching sheet, Chinese Journal of Physics 66 : 258-268.

Wang, C. Y. (2002). Flow due to a stretching boundary with partial slip an exact solution of the Navier-Stokes equations. Chem. Eng. Sci, 57(17): 3745-3747.

Sophus, L., Ackerman, M. (1976). Sophus Lies 1884 Differential Invariant Paper, Math Sci. Press.

Sreenivasulu, P., Poornima, T. and Reddy, N. B. (2019). Influence of Joule Heating and Non-Linear Radiation on MHD 3D Dissipating Flow of Casson Nanofluid past a Non-Linear Stretching Sheet, Nonlinear Engineering, 8: 661-672

Sumalatha, C., Bandari, S. (2015). Effects of Radiations and Heat Source/Sink on a Casson Fluid Flow over Nonlinear Stretching Sheet. World Journal of Mechanics. 5:257-265.

Zaimi, K., Ishak, A. (2016). Stagnation-point flow towards a stretching vertical sheet with slip effects. MDPI Mathematics, 4(2): 27.

Zakir, U., Zaman, G. (2017). Lie group analysis of magnetohydrodynamic tangent hyperbolic fluid flow towards a stretching sheet with slip conditions. Heliyon, 3 e00443.

Zakir, U., Zamana, G., Ishak, A., (2020). Magnetohydrodynamic tangent hyperbolic fluid flow past a stretching sheet. Chinese Journal of Physics, 66: 258-268.